Observations of Barotropic Oscillations and Their Influence on Mixing in the Faroe Bank Channel Overflow Region

E. DARELIUS, J. E. ULLGREN, AND I. FER

Geophysical Institute, University of Bergen, Bergen, Norway

(Manuscript received 25 March 2013, in final form 12 April 2013)

ABSTRACT

Observations of hydrography, currents, and microstructure are presented together with sea surface height (SSH) patterns from concurrent satellite tracks to describe the subinertial oscillations in the region downstream of the Faroe Bank Channel overflow. Energetic oscillations with a dominant 3–5-day period have previously been observed in the dense bottom layer and found to be consistent with topographic Rossby waves. Here, the authors present evidence that the oscillations extend over the whole water column and are connected to a wave-like pattern in SSH along the continental slope. The waves are observed in two satellite tracks running parallel to the slope and indicate a wavelength of 50–75 km, an amplitude of about 5 cm, and a phase speed of 15–20 cm s^{-1}. The pattern extends at least 450 km along the slope. Repeat occupations of a section through a 4-day period show a barotropic velocity anomaly that is associated with an increase in plume transport [from 0.5 to 2.5 Sv (1 Sv $\equiv 10^6\,m^3\,s^{-1}$)] and interface height (from 100 to 200 m) as well as changes in dissipation rates and mixing. Estimates of entrainment velocity w_E vary with a factor of 10^2 over the oscillation period, and there is an inverse relation between w_E and plume thickness, that is, mixing is most intense when the dense bottom layer is thin. High values of w_E coincide with a large percentage of critical Richardson numbers in the interfacial layer. The rotational motion, or the horizontal "stirring," is observed to bring water from the south, traceable because of its low oxygen concentrations, into the plume.

1. Introduction

The Faroe Bank Channel (FBC) is, with a sill depth of 860 m, the deepest passage in the Greenland–Scotland ridge and it accommodates an outflow of 1.7 Sv (1 Sv $\equiv 10^6\,m^3\,s^{-1}$) dense, cold ($T < 3$°C) water from the Nordic seas toward the North Atlantic Ocean (Hansen and Østerhus 2007). Upon leaving the channel, the dense water descends the continental slope, entraining and mixing with the ambient water to eventually become North Atlantic Deep Water (NADW).

The region downstream of the FBC sill is characterized by high sea level variability (Høyer and Quadfasel 2001) and current meter records from the plume area show high mesoscale variability (Darelius et al. 2011, hereafter D11; Geyer et al. 2006, hereafter G06). The flow of dense water along the slope is generally better described as boluses or domes of cold water traveling along the slope than as a continuous plume. These boluses are typically 100–200 m thick, they occur with a periodicity of 2.5–6 days, and the flux of dense water has been observed to increase from 0.5 to 2 Sv as they move past a mooring array (D11). The boluses are associated with strong oscillations in the velocity fields and they are suggested to be linked to trains of alternating anticyclonic and cyclonic eddies, whose properties broadly agree with topographic Rossby waves (TRWs; Rhines 1970). Observations indicate that the TRWs have an along-slope wavelength of 75–180 km and a phase speed between 0.25 and 0.60 m s^{-1} (D11). The anticyclonic eddies are associated with the boluses (i.e., with high plume transport and low temperatures) and the cyclones with the warmer, intermediate periods (D11). The center of the eddies is conjectured to lie shallower than the 800-m isobath and to have a cross-slope length scale larger than the plume/boluses.

Levels of mixing and entrainment are high in the area downstream of the FBC sill (Fer et al. 2010; Beaird et al. 2012). Model studies of dense plumes show that eddies influence vertical mixing (Seim et al. 2010), and it has been shown from observations in the Denmark Strait overflow that eddies increase horizontal mixing through

Corresponding author address: E. Darelius, Geophysical Institute, University of Bergen, Alleg. 70, 5007 Bergen, Norway.
E-mail: darelius@gfi.uib.no

DOI: 10.1175/JPO-D-13-059.1

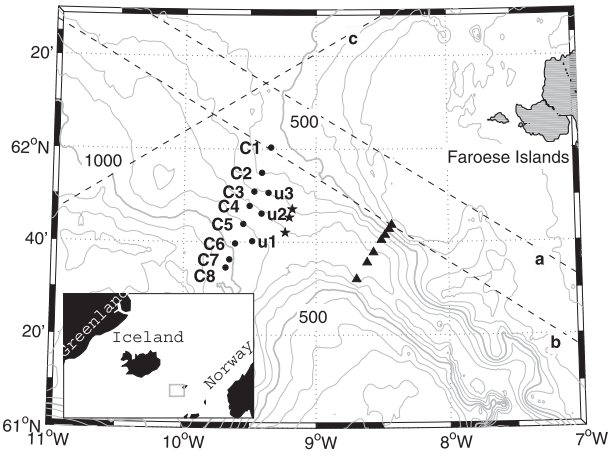

FIG. 1. Map showing the bathymetry of the study region together with the position of CTD/LADCP/VMP sections A (triangles), B (stars), and C (circles) and satellite tracks a, b, and c. Isobaths (GEBCO 2012) are shown every 100 m with the 500- and 1000-m isobaths drawn with thick lines. The inset shows the location of the study area (gray rectangle).

stirring (Voet and Quadfasel 2010). The FBC outflow represents roughly one-third of the total overflow across the Greenland–Scotland ridge and mechanisms influencing the mixing in this region will hence have consequences for the final properties of the produced NADW. In this paper, we present new observational data from a repeated section (hydrography, currents, and microstructure) revealing the barotropic nature of the eddies/waves and their influence on entrainment and mixing.

2. Data and methods

a. Cruise observations

Observations of hydrography, currents, and microstructure were made during a cruise with research vessel *Håkon Mosby* in June 2012. Stations along section C, 150 km downstream of the FBC sill and perpendicular to the slope (Fig. 1), were occupied repeatedly between 1157 UTC 1 June and 1032 UTC 4 June 2012. During this period, the section was occupied (fully or partly) five times, and the measurements were then continued at stations C4, C5, and u2 (hereafter triangle T1) until 2212 UTC 5 June, giving a total of nine profiles at these stations. In total 57 profiles of hydrography and velocity were collected with a conductivity–temperature–depth (CTD; SBE911+) package equipped with down and upward looking lowered acoustic Doppler current profilers (LADCPs; 300-kHz Workhorse). Each CTD cast was, when the weather permitted, directly followed by a cast using a vertical microstructure profiler (VMP; Rockland Scientific International) giving a total of 42 casts. The VMP is equipped with accurate CTD sensors and a pair of microstructure shear probes used for measuring the dissipation rate of turbulent kinetic energy ε. The processing of the microstructure data follows Fer (2009). The velocity data have been detided using the Earth & Space Research (ESR)/Oregon State University (OSU) tidal model version European Shelves (Egbert et al. 2010), and when velocity anomalies are presented, the survey-mean current from that station and depth interval has been removed. The tidal velocities were up to 15 cm s^{-1}.

b. Satellite altimetry

Satellites providing altimetry data (*Jason-1C* and *-2*) passed over the study region three times during the observation period: tracks a (1501 UTC 2 June) and b (1437 UTC 4 June) running roughly parallel to the 600- and 700-m isobaths, respectively, and track c (1003 UTC 3 June), which crosses the slope with an about 30° angle (see Fig. 1 for location). Along-track sea surface height (SSH) data were downloaded from Radar Altimeter Database System (RADS; http://rads.tudelft.nl/rads/rads.shtml), and a 5-point running Hanning filter was applied along the tracks to remove small-scale disturbances and noise. The component of the geostrophic velocity perpendicular to the track that is associated with the sea surface slope between two neighboring points is estimated from

$$v_g = -\frac{g}{f}\frac{\Delta \mathrm{SSH}}{\Delta x} \tag{1}$$

and the vorticity along the track is estimated from

$$\xi = 2 \times \frac{\partial v_g}{\partial x}, \tag{2}$$

under the assumption that the motion is circular.

3. Results

During the time of observations, the dense overflow plume was evident at section C between the 600- and 900-m isobaths as a cold bottom layer, extending 100–200 m above the bottom and flowing along the slope with a mean velocity of about 30–40 cm s^{-1} at the central stations (Figs. 2a,b). The dissipation rates in the upper layer were relatively low (10^{-9} W kg^{-1}) while turbulence levels increased within the plume, as described previously by Fer et al. (2010), typically reaching a maximum of 10^{-6}–10^{-5} W kg^{-1} in the bottom boundary layer and showing a local, slightly lower, maximum in the plume interface (Figs. 2c,d). The plume thickness,

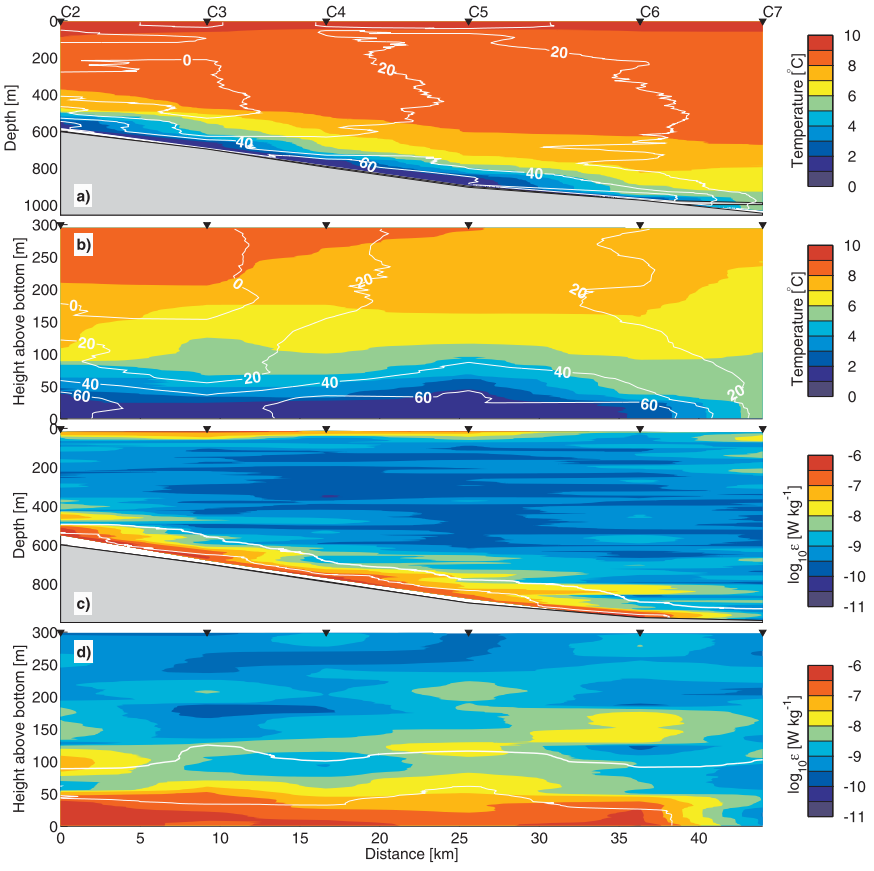

FIG. 2. Sections of (a),(b) temperature (°C) and (c),(d) dissipation rate ε (W kg^{-1}) from the second occupation of section C (0320–1300 UTC 2 Jun 2012) where (a),(c) the full depth and (b),(d) the bottommost 300 m are shown. White contours in (a) show along-slope/across-section velocity (cm s^{-1}) while contours in (c),(d) show the position of the 3° (thin line) and 6°C (thick line) isotherms.

velocity, its horizontal extent, and location on the slope vary considerably during the measurement period.

a. Velocity anomalies and plume thickness

Throughout the observation period, there was a strong (25–50 cm s^{-1}) and variable current in the upper layer. The velocity vectors were observed to rotate counterclockwise at the deeper stations (>800 m, C5–7 and u2–3), completing 0.5–0.75 rotations in 62 h (Fig. 3a) and thus suggesting a periodicity of 3.5–5 days. At the shallow stations (<700 m, C2–3 and u1) the velocity vector rotated clockwise. The signal is relatively homogenous in the vertical, above the bottom 200 m where the flow is highly affected by the plume (Fig. 3b), and there is no significant change in the amplitude of the velocity oscillations with depth (Fig. 3c). There is a tendency, especially at the shallower stations, for velocity anomalies to be larger in the across-slope direction than in the along-slope direction.

Figure 4a shows the time evolution of temperature and currents at station C4, representative for the central stations in the section. The plume thickness, defined as the height above bottom of the 6°C isotherm, increases from about 100 to over 200 m during the oscillation period. The plume is thickest when the velocity induced by the oscillation in the upper layer is directed down the slope, parallel to the section. This is also when the difference between the velocity in the upper layer and the velocity of the plume ΔU is smallest and when the lowest bottom temperatures are observed (Fig. 4b,e).

b. Vorticity

The observed time series of relative vorticity $\xi = \Delta \times \mathbf{V} \approx \Delta v/\Delta x - \Delta u/\Delta y$ estimated using upper-layer velocity anomalies from triangle T1 (C4, C5, and u2) is shown in Fig. 4b. The vorticity at T1 oscillates around zero with an apparent period of roughly 70 h, where positive values indicate cyclonic and negative values anticyclonic motion,

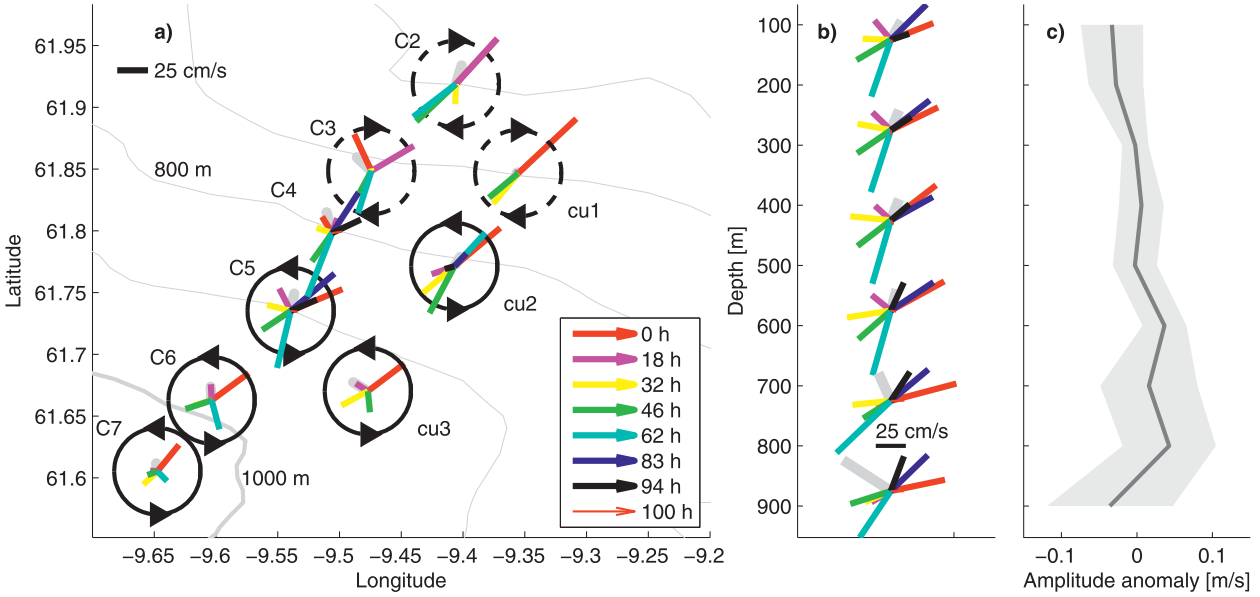

FIG. 3. (a) Depth-averaged, upper-layer velocity anomalies (50–300 m) from LADCP at section C. (b) Velocity anomalies (depth averaged in 100-m bins) at station C5. (c) Survey-mean profile of velocity amplitude anomaly calculated as the deviation from the vertical-mean speed at each occupation. The gray envelope is one std dev. The colors in (a),(b) indicate time since the first occupation according to the scale in (a). Thick light gray arrows in (a),(b) show the survey-mean current. Circles and arrows in (a) show the local direction of rotation (dashed line = clockwise rotation; solid line = counterclockwise rotation). Isobaths are shown in 100-m intervals and the scale of velocity is shown in the top left corner in (a) and in the bottom corner in (b).

respectively. A similar oscillation in vorticity was observed by D11, who found a significant, positive correlation between bottom temperature and vorticity (based on 3-month-long mooring records). The temperature record presented here (Figs. 4a,b) suggests a similar relation at C4, but this is not generally true for all stations.

c. *Plume transport*

The transport of water colder than T°C through the section is estimated (for the five sections only) using the detided velocity profiles from $Q(T) = \sum_{i=1}^{n}\sum_{z=0}^{z_T} L_i u_i(z)\Delta z$, where n is the number of stations in the section, z_T is the height above bottom of the T°C isotherm, L_i is the representative width of the station, u_i is the velocity component perpendicular to the section (positive to the northwest), and $\Delta z = 8$ m is the resolution of the LADCP measurements. The velocity oscillations are associated with large changes in plume transport: the transport of water colder than 3°C increases from 0.5 to 2.5 Sv over the first five occupations, roughly covering half of a period (Fig. 4c). Water colder than 0°C is only present during the two last occupations of the section.

d. *Mixing and entrainment*

The entrainment velocity w_E calculated from the observed dissipation rates following Arneborg et al. (2007), oscillates between 10^{-6} and 10^{-4} m s^{-1}, that is, by a factor of 10^2 during the observation period (Fig. 4d). High values of w_E occur when a large portion of the plume show small (<1) gradient Richardson numbers Ri (Fig. 4d),

$$\mathrm{Ri} \approx \frac{\dfrac{-g}{\rho_0}\dfrac{\Delta\sigma_\Theta}{\Delta z}}{\left(\dfrac{\Delta u}{\Delta z}\right)^2 + \left(\dfrac{\Delta v}{\Delta z}\right)^2}. \qquad (3)$$

At section C, and partly at B (see Fig. 1), large entrainment velocities are associated with a thin plume, and vice versa, while there is no such connection at the sill (not shown).

Figure 5 shows how the motion caused by the eddies brings water from the south, easily identified by a relatively strong oxygen minimum (down to ~4.7 ml l^{-1} compared to background levels of about 5.9 ml l^{-1}), into the plume interfacial layer. The concentration of dissolved oxygen is higher in the water above the interfacial layer and within the plume below. The oxygen minimum, which is not observed at the sill crest (section A, Fig. 1), must thus be advected horizontally, or "stirred," into the plume region.

e. *Altimetry*

SSH inferred from satellite altimetry along the tracks a and b (aligned with the slope, Fig. 1) shows a wave

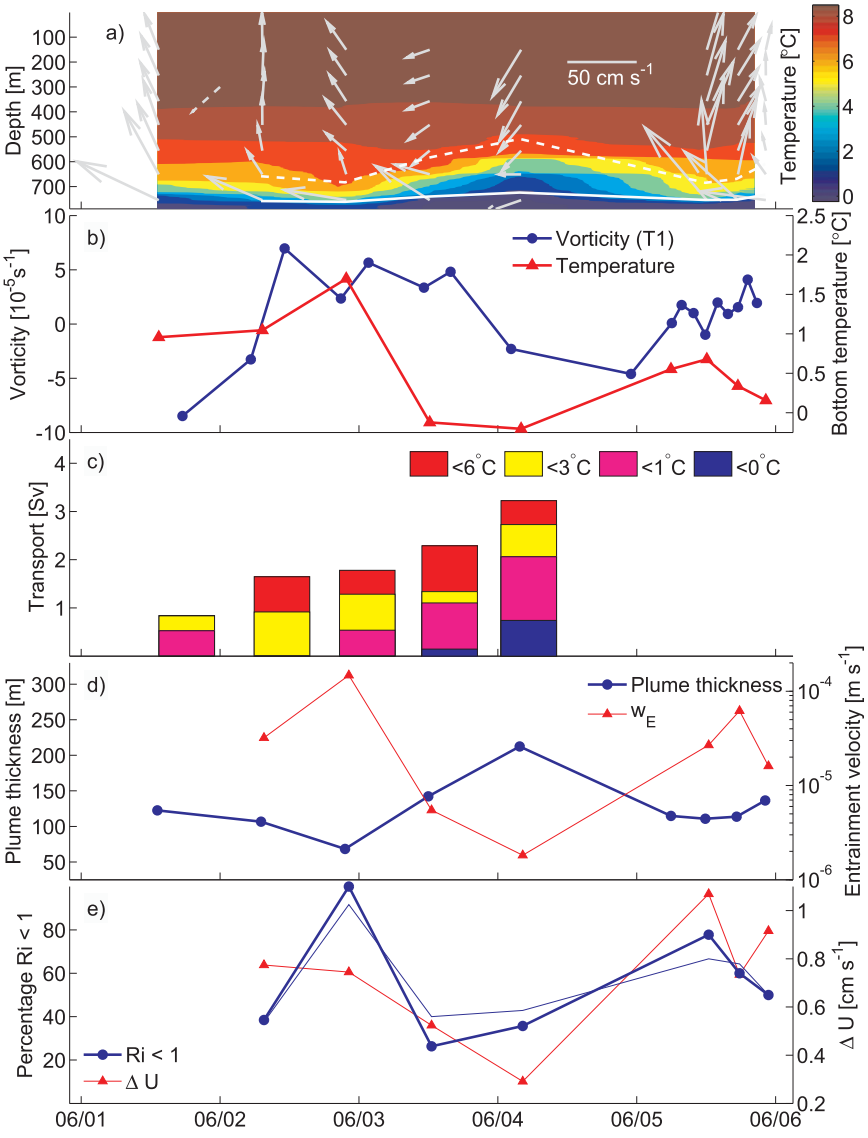

FIG. 4. (a) Hovmöller diagram of temperature at station C4. Horizontal currents (gray vectors) and the depth of the boundary layer (solid white line) and interfacial layer (dashed white line) following definitions of Fer et al. (2010) are superimposed. The orientation of section C, roughly orthogonal to the isobaths, is indicated with dashed gray lines. Time series of (b) vorticity estimated from triangle T1 and bottom temperature, (c) transport across the section C in temperature classes, (d) height of the 6°C isotherm (defined as the plume thickness) and entrainment velocity, and (e) the percentage of Ri < 1 in interface (thick blue lines) and over the plume (thin blue lines) and of the magnitude of the vector difference between the maximum plume velocity $\overline{U_p}$ and the velocity of the upper layer $\overline{U_u}$, that is, $\Delta U = |\overline{U_p} - \overline{U_u}|$. When not stated otherwise, observations are from station C4.

pattern with an amplitude of 5 cm and a wavelength of 50–75 km, traveling along the slope so that the two tracks, separated in time by two days, are perfectly out of phase (Fig. 6a). This suggests a periodicity of 4 days or about 100 h, in general agreement with the observations from section C, and an along-slope phase speed of 15–20 cm s^{-1}. The component of the geostrophic currents perpendicular to the track that is associated with the sloping sea surface [from Eq. (1)] agrees with the observed velocity anomalies in direction and, to within a factor of 2, in magnitude (Fig. 6d). Estimates of vorticity along the track [from Eq. (2)] compare to the time series of vorticity from T1, when the time axis is scaled with the observed phase speed (Fig. 6b).

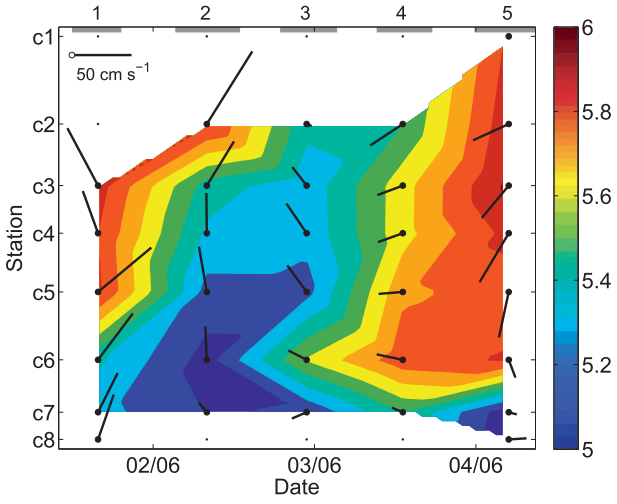

FIG. 5. Oxygen concentration (ml l^{-1}) averaged in the interfacial layer, here defined as the potential temperature range 3°–8°C, as a function of time and latitude along section C. Black vectors show horizontal current averaged over the upper 50–300 m. All measurements are shown at the mean time of occupation from 1 to 5 of the section. The duration of each occupation is shown by the gray lines at the top of the plot.

4. Discussion

Independent threads of evidence are presented showing barotropic, subinertial oscillations, which modulate mixing and induce stirring in the Faroe Bank Channel overflow region. The oscillations are associated with anomalies of about 5 cm in SSH along the continental slope with a wavelength of 50–75 km, a period of about four days and thus a phase velocity of 15–20 cm s^{-1}. This is slightly lower than previous estimates from the same area, where the along-slope phase velocity ranges between 25 and 60 cm s^{-1} and wavelength ranges between 75 and 180 km (D11, G06). The period, induced flow, and vorticity inferred from altimetry agree with the results from the sections worked during the cruise. The observations are, as suggested by D11, generally consistent with TRWs.

The mechanisms for oscillations and the preference for the observed period are beyond the scope of this study. We can, however, speculate on one possibility—that the TRWs are generated as a result of the growth and decay of the slope current meanders observed in the Faroe Shetland Channel, which have comparable time and length scales (Sherwin et al. 2006). Such a coupling has previously been proposed by Pickart (1995) relating Gulf Stream meanders and TRWs observed along the continental slope of the Mid-Atlantic Bight. It requires that the topographic β dominates over the planetary β and that the isobaths are oriented with a northward component, both of which are fulfilled in the Faroe Shetland Channel.

The wave signal in SSH extends at least 460 km westward along the slope, that is, as long as the satellite tracks are parallel to the slope (the isobaths curve northward and deviate from the tracks at about 13°W, see Fig. 6). Contrary to our observations, increased SSH variability, previously reported 50 km downstream of the sill, did not persist at greater distances from the sill (Høyer and Quadfasel 2001). The spindown time of TRWs in this region was estimated by D11 to be 3–7 days using vertical eddy viscosity estimates from the highly turbulent plume region ($A_z = 10^{-2}$ m^2 s^{-1}; Fer et al. 2010). The wave reported here would require 26 days to travel across the slope with the observed phase velocity, suggesting an effective viscosity less than 10^{-3} m^2 s^{-1}. This one order of magnitude reduction in the eddy viscosity is plausible since the turbulence levels drop off drastically once the waves travel out of the highly turbulent region downstream of the FBC sill (Beaird et al. 2012).

The observed oscillations, probably caused by TRWs, affect the FBC overflow plume dynamics and mixing. They induce, in addition to large spatial variability in the FBC overflow mixing and entrainment (Beaird et al. 2012; Fer et al. 2010; Mauritzen et al. 2005), large temporal variability with w_E changing with a factor of 10^2 during an oscillation period. Somewhat counterintuitively, low mixing rates coincide with large plume thicknesses. This is likely related to changes in the bulk shear, here expressed by ΔU, between the plume and the ambient water. When the velocity induced by the oscillation in the upper layer is comparable with that of the plume, that is, when ΔU is at its minimum, the plume thickens or forms domes. At the same time, mixing is reduced, since the bulk shear and thus the energy available for shear-induced mixing decreases. This allows for dense overflow water in the center of the domes to flow along the slope relatively unmodified. As the plume thins in response to positive vorticity and increasing ΔU, the entrainment velocity significantly increases and nearly the entire overflow layer is associated with Ri < 1. The increased friction will allow the plume to cross the isobaths, increasing its rate of descent. The dynamical process linking the barotropic flow to changes in plume thickness is unknown and deserves further studies.

Numerical models of the FBC overflow tend to develop eddies with a periodicity similar to the observed oscillations (e.g., Ezer 2006; Seim et al. 2010), and modeled dissipation rates have been shown to vary with a factor of 2–10 as an eddy passes (Seim et al. 2010). In accordance with observations, low dissipation rates coincide with large plume thickness. The effect of the observed horizontal stirring induced by the waves remains to be quantified. The observed waves can be expected to modify the vertical mixing and induce horizontal stirring

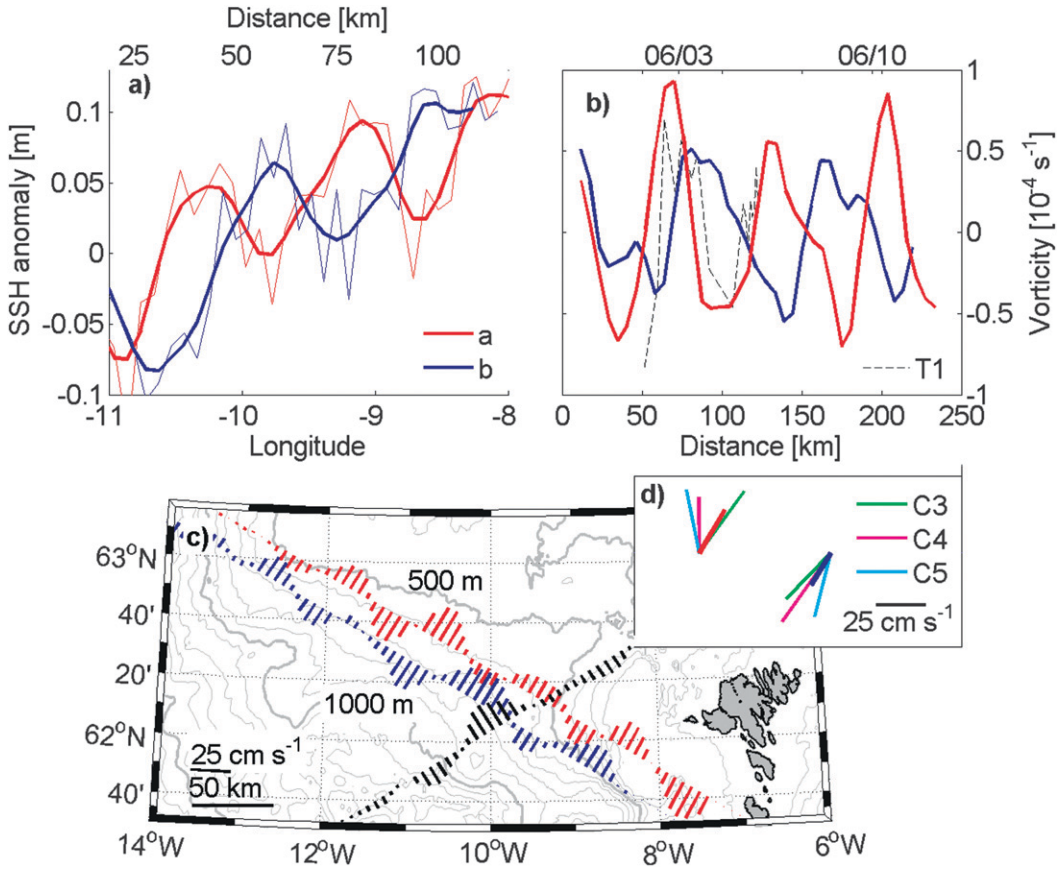

FIG. 6. (a) SSH anomaly along the tracks a and b as raw (thin line) and low-pass filtered (thick line) data. (b) Vorticity as a function of distance estimated from SSH along the tracks a and b and vorticity as a function of time from triangle T1. The time (top x axis) is scaled using the observed speed of phase propagation (20 cm s^{-1}) to agree with the distance (bottom x axis). (c) Map showing the component of the geostrophic velocity perpendicular to the satellite tracks (a = red, b = blue, and c = black) associated with the SSH variability. The velocity and length scales are given at the bottom left corner of the panel. (d) Velocity anomalies in the upper layer at stations C3–5 from the occupation closest in time to the satellite passages and the across-track velocity component inferred from SSH from the location closest in space to section C. The SSH velocities are color-coded according to the scale in (a) and the velocity scale is given at the bottom right corner of the panel.

of the plume water, not only locally in the study area, but during much of its descent along the continental slope.

Acknowledgments. The authors wish to thank the crew, technicians, and students involved in the fieldwork. This study was funded by the Research council of Norway through the project Faroe Bank Channel Overflow: Dynamics and Mixing.

REFERENCES

Arneborg, L., V. Fiekas, L. Umlauf, and H. Burchard, 2007: Gravity current dynamics and entrainment—A process study based on observations in the Arkona Basin. *J. Phys. Oceanogr.,* **37,** 2094–2113.

Beaird, N., I. Fer, P. Rhines, and C. Eriksen, 2012: Dissipation of turbulent kinetic energy inferred from Seagliders: An application to the eastern Nordic Seas overflows. *J. Phys. Oceanogr.,* **42,** 2268–2282.

Darelius, E., I. Fer, and D. Quadfasel, 2011: Faroe Bank Channel overflow: Mesoscale variability. *J. Phys. Oceanogr.,* **41,** 2137–2154.

Egbert, G. D., S. Y. Erofeeva, and R. D. Ray, 2010: Assimilation of altimetry data for nonlinear shallow-water tides: Quarter-diurnal tides of the Northwest European Shelf. *Cont. Shelf Res.,* **30,** 668–679, doi:10.1016/j.csr.2009.10.011.

Ezer, T., 2006: Topographic influence on overflow dynamics: Idealized numerical simulations and the Faroe Bank Channel overflow. *J. Geophys. Res.,* **111,** C02002, doi:10.1029/2005JC003195.

Fer, I., 2009: Weak vertical diffusion allows maintenace of cold halocline in the central Arctic. *Atmos. Oceanic Sci. Lett.,* **2,** 148–152.

——, G. Voet, K. S. Seim, B. Rudels, and K. Latarius, 2010: Intense mixing of the Faroe Bank Channel overflow. *Geophys. Res. Lett.,* **37,** L02604, doi:10.1029/2009GL041924.

GEBCO, cited 2012: General Bathymetric Chart of the Oceans (GEBCO). [Available online at www.gebco.net.]

Geyer, F., S. Østerhus, B. Hansen, and D. Quadfasel, 2006: Observations of highly regular oscillations in the overflow plume downstream of the Faroe Bank Channel. *J. Geophys. Res.,* **111,** C12020, doi:10.1029/2006JC003693.

Hansen, B., and S. Østerhus, 2007: Faroe Bank Channel overflow 1995-2005. *Prog. Oceanogr.,* **75,** 817–856.

Høyer, J. L., and D. Quadfasel, 2001: Detection of deep overflows with satellite altimetry. *Geophys. Res. Lett.,* **28,** 1611–1614.

Mauritzen, C., J. Price, T. Sanford, and D. Torres, 2005: Circulation and mixing in the Faroese Channels. *Deep-Sea Res. I,* **52,** 883–913.

Pickart, R., 1995: Gulf stream-generated topographic Rossby waves. *J. Phys. Oceanogr.,* **25,** 574–586.

Rhines, P., 1970: Edge, bottom, and Rossby waves in a rotating stratified fluid. *J. Fluid Mech.,* **69,** 273–302.

Seim, K., I. Fer, and J. Berntsen, 2010: Regional simulations of the Faroe Bank Channel overflow using a sigma-coordinate ocean model. *Ocean Modell.,* **35** (1–2), 31–44.

Sherwin, T. J., M. O. Williams, W. R. Turrell, S. L. Hughes, and P. I. Miller, 2006: A description and analysis of mesoscale variability in the Faroe-Shetland Channel. *J. Geophys. Res.,* **111,** C03003, doi:10.1029/2005JC002867.

Voet, G., and D. Quadfasel, 2010: Entrainment in the Denmark Strait overflow plume by meso-scale eddies. *Ocean Sci.,* **6,** 301–310.